Topological defects of optical indicatrix orientation associated with the edge structural dislocations in crystals

Savaryn V., Vasylkiv Yu., Skab I. and Vlokh R.

Vlokh Institute of Physical Optics, 23 Dragomanov Street, 79005 Lviv, Ukraine, vlokh@ifo.lviv.ua

Received: 19.06.2015

Abstract. We have analyzed the effect of edge structural dislocations in solid-crystalline structures on the topology of optical indicatrix parameters. It has been found that consideration of strict boundary conditions leads to zeroing of the stress tensor components in the vicinity of dislocation core. Subsequently, piezooptically induced birefringence in the vicinity of the dislocation core conditions the appearance of optical vortices around this core. Basing on our analysis, we have demonstrated that, even with small Burgers vectors and intermediate values of piezooptic coefficients, the edge dislocation can be detected in the polarized light using optical microscopes.

Keywords: crystalline structure, edge dislocations, optical indicatrix, topological defects

PACS: 42.50.Tx, 78.20.Fm, 42.50.-p, 78.20.hb, 61.50.-f, 61.72.Ff
UDC: 535.5+544.022.341.1

1. Introduction

Topological defects (TD) of optical indicatrix (OI) orientation represent an important tool for creating defects of light wave front, which induce optical vortices [1–4]. Optical beams bearing the vortices (or orbital angular momentum abbreviated hereafter as OAM) have found their applications in a number of novel branches of science, e.g. information processing [5], quantum cryptography [6, 7], and quantum teleportation [8]. They can also be used while manipulating microparticles [9]. Furthermore, discovery of the beams carrying nonzero OAMs has given a start for such new branches of optics as a singular optics [10].

The TDs of OI orientation or, in more exact terms, the structural defects in liquid crystals probably have for the first time been used for optical vortex generation by the authors of Refs. [11–14]. As follows from these works the electric field component of the outgoing electromagnetic wave at the spin angular momentum (SAM) to OAM conversion process, in the case when the beam propagates through a system consisting of a right-handed circular polarizer, a sample with the liquid crystal structural defect, and a left-handed circular analyzer can be determined by the equation:

$$E^{out}(\varphi) = E_a \cos\frac{\Delta\Gamma}{2}\begin{bmatrix}1\\ i\end{bmatrix} + iE_a \sin\frac{\Delta\Gamma}{2}\exp\left(i2q\varphi + i2\alpha_0\right)\begin{bmatrix}1\\ -i\end{bmatrix}, \quad (1)$$

where $m = 2q$ denotes the number of helicoidal lobes in the helical electromagnetic mode, q the strength of the liquid-crystalline defect, $\Delta\Gamma$ the optical phase difference, E_a the incident plane-wave amplitude, α_0 the angle of director orientation at $\varphi = 0$, and $E^{out}(\varphi)$ the outgoing wave amplitude.

The first term in the Eq. (1) describes the outgoing plane wave with the same SAM value as for the incident wave ($-\hbar$), while the second term corresponds to a helical mode bearing the OAM. The phase front of the incident beam is taken to be approximately plane, while the SAM of the incident photons is equal to $S^{inc} = -\hbar$. The requirement of conservation of the total angular momentum leads to the following relation for the angular momentum transformation:

$$J^{inc} = J^{out} + M\,, \tag{2}$$

where $J^{inc} = S^{inc} = -\hbar$ means the total angular momentum for the incident photon, $J^{out} = L^{out} + S^{out} = -2q\hbar + \hbar = 0$ the total angular momentum for the emergent photon ($S^{out} = +\hbar$, $L^{out} = -2q\hbar$), and L^{out} the OAM for that photon. Thus, the mechanical angular momentum transferred to a material medium due to the Beth effect [15] is equal to $M = -\hbar$. As seen from Eq. (1), the charge of the optical vortex m is determined by the strength of the liquid crystal defect q. As it is seen from Eq.(1) in the case of liquid crystals, the strength of the structural defect of the director orientation is equal to the strength of the TD of OI orientation. However in the solid transparent inhomogeneous materials the strength of TD of OI orientation is unique parameter by which the charge of the vortex can be defined. Summing up, the liquid-crystal structural defects lead to appearance of defects, or singularities, of the wave front and, thus, to appearance of the optical vortices.

Recently we have shown [16, 17] that dislocations in solid crystalline materials also lead to appearance of dislocations of the phase front. When compared with the liquid crystals, this process is more complicated. The dislocations produce specific spatial distributions of mechanical stress around their cores, while the stresses induce the changes in the refractive indices via a piezooptic effect, thus resulting in the appearance of TDs of OI orientation. Moreover, the elastic fields of edge and screw dislocations act upon the refractive indices in a different manner. In particular, the screw structural dislocations produce the TDs with the strength equal to ½ and so singly charged optical vortices, while the edge dislocations impose the TDs with the strength equal to 1 and doubly charged optical vortices.

In the studies [16, 17] we have analyzed the spatial distribution of the OI angle produced by the elastic field around the edge dislocation core, basing on the simplified relations [18, 19] for the stress tensor components:

$$\begin{aligned}
&\sigma_1 = -\frac{G_1 b}{2\pi(1-\mu_1)}\frac{Y(3X^2+Y^2)}{(X^2+Y^2)^2},\ \sigma_2 = \frac{G_2 b}{2\pi(1-\mu_2)}\frac{Y(X^2-Y^2)}{(X^2+Y^2)^2},\\
&\sigma_3 = \mu_3(\sigma_1+\sigma_2),\ \sigma_6 = \frac{G_3 b}{2\pi(1-\mu_3)}\frac{X(X^2-Y^2)}{(X^2+Y^2)^2},\\
&\sigma_4 = \sigma_5 = 0,
\end{aligned} \tag{3}$$

where G_k are the shear modules, μ_l the Poisson ratios (k, l = 1, 2, 3), X and Y the coordinates, and $\boldsymbol{b}$ denotes the Burgers vector. Eqs. (3) are valid when the edge dislocation with the Burgers vector $\boldsymbol{b}$ parallel to the direction [100] and the dislocation line parallel to [001] are dealt with. The module of the Burgers vector is then equal to

$$|b| = \frac{a}{2}\sqrt{h^2+k^2+l^2} = \frac{a}{2}\,, \tag{4}$$

where a is the lattice parameter and h, k and l the Miller indices. Here [$hk\ell$] denotes the direction

associated with the basis of direct-lattice vectors, which is perpendicular to the lattice plane (*hkl*). Note that this formula can be obtained from the general relations of Refs. [18–20], provided that the radius of the dislocation core becomes zero and the crystalline sample is supposed to have infinite size. In other words, the boundary conditions are not considered while deriving Eqs. (3).

Since one can hope to detect the TDs of OI orientation, and the resulting optical vortices, with optical microscopic observations, a simple new method for revealing structural dislocations can, in principle, be developed on this basis. However, knowledge on the exact spatial distribution of OI parameters is then needed. The aim of the present work is to analyze the distribution of OI parameters, basing on consideration of general equations for the stress distribution around the core of the edge dislocations in crystals.

2. Results of analysis

Below we will consider the edge dislocation appearing in the crystals that belong to both the cubic (the point symmetry groups m3m, 432 and $\bar{4}3m$) and trigonal (the groups 3m, 32 and $\bar{3}m$) systems, with the Burgers vector parallel to the [010] axis and the dislocation line parallel to the [001] axis. Since, from the viewpoint of symmetry, the elastic and piezooptic properties of the crystals belonging to those cubic and trigonal groups are the same, we perform our analysis only for the example cases of NaCl (the group m3m) and $LiNbO_3$ (the group 3m).

Let us analyze the general relations for the stress tensor components taken from Ref. [18, 20] and written in the right-handed cylindrical coordinate system φ, r, Z:

$$\sigma_{rr} = \frac{Gb}{2\pi(1-\mu)}\frac{1}{r}\left[1-\frac{\left(\frac{r}{R}\right)^2+\left(\frac{r_0}{r}\right)^2}{1+\left(\frac{r_0}{R}\right)^2}\right]\sin\varphi,\ \ \sigma_{\varphi\varphi} = \frac{Gb}{2\pi(1-\mu)}\frac{1}{r}\left[1-\frac{3\left(\frac{r}{R}\right)^2-\left(\frac{r_0}{r}\right)^2}{1+\left(\frac{r_0}{R}\right)^2}\right]\sin\varphi,$$
$$\sigma_{33} = \frac{Gb\mu}{\pi(1-\mu)}\frac{1}{r}\left[1-\frac{2\left(\frac{r}{R}\right)^2}{1+\left(\frac{r_0}{R}\right)^2}\right]\sin\varphi,\ \ \sigma_{r\varphi} = \frac{Gb}{2\pi(1-\mu)}\frac{1}{r}\left[1-\frac{\left(\frac{r}{R}\right)^2+\left(\frac{r_0}{r}\right)^2}{1+\left(\frac{r_0}{R}\right)^2}\right]\cos\varphi, \quad (5)$$

where R is the radius of a crystalline cylinder and r_0 the radius of the dislocation core. As shown in Ref. [20], these relations are valid for a hollow cylinder with its bases subjected to loading. On the other hand, the complete conditions have to include the state at which the bases of the cylinder are free of loading and the surfaces at $r = R$ and $r = r_0$ are free of stresses.

As follows from the analysis [20], the solution of the latter problem, most probably, is impossible. In Ref. [20], the following boundary conditions have been used: $\sigma_1, \sigma_6 = 0\big|_{r_0,\, R=0}$, $\sigma_2 \neq 0\big|_{r_0,\, R=0}$ and $\sigma_3 \neq 0\big|_{Z=\pm L/2}$, with L being the height of the cylinder. Then, using the relations

$$\begin{aligned}
\sigma_1 &= \cos^2\varphi\sigma_{rr} + \sin^2\varphi\sigma_{\varphi\varphi} - \sin 2\varphi\sigma_{r\varphi},\\
\sigma_2 &= \sin^2\varphi\sigma_{rr} + \cos^2\varphi\sigma_{\varphi\varphi} + \sin 2\varphi\sigma_{r\varphi},\\
\sigma_6 &= \frac{1}{2}\sin 2\varphi(\sigma_{rr} - \sigma_{\varphi\varphi}) + \cos 2\varphi\sigma_{r\varphi}.
\end{aligned} \quad (6)$$

one can rewrite Eqs. (5) in the Cartesian coordinate system as

$$\sigma_1 = \frac{Gb}{2\pi(1-\mu)}\frac{Y}{\left(X^2+Y^2\right)^2}\times$$
$$\left[Y^2\left(1-\frac{3\left(\frac{X^2+Y^2}{R^2}\right)-\left(\frac{r_0^2}{X^2+Y^2}\right)}{1+\left(\frac{r_0}{R}\right)^2}\right)-X^2\left(1-\frac{\left(\frac{X^2+Y^2}{R^2}\right)+\left(\frac{r_0^2}{X^2+Y^2}\right)}{1+\left(\frac{r_0}{R}\right)^2}\right)\right],$$
$$\sigma_2 = \frac{Gb}{2\pi(1-\mu)}\frac{Y}{\left(X^2+Y^2\right)^2}\times \tag{7}$$
$$\left[\left(2X^2+Y^2\right)\left(1-\frac{\left(\frac{X^2+Y^2}{R^2}\right)+\left(\frac{r_0^2}{X^2+Y^2}\right)}{1+\left(\frac{r_0}{R}\right)^2}\right)+X^2\left(1-\frac{3\left(\frac{X^2+Y^2}{R^2}\right)-\left(\frac{r_0^2}{X^2+Y^2}\right)}{1+\left(\frac{r_0}{R}\right)^2}\right)\right].$$

Here we neglect the stress tensor component σ_3, since it does not affect the birefringence Δn_{12} and the angle of OI orientation ξ_3 (see below). At $r_0 = 0$, Eqs. (7) may be represented as

$$\sigma_1 = \frac{Gb}{2\pi(1-\mu)R^2}\frac{Y}{\left(X^2+Y^2\right)^2}\left[Y^2\left(R^2-3\left(X^2+Y^2\right)\right)-X^2\left(R^2-\left(X^2+Y^2\right)\right)\right],$$
$$\sigma_2 = \frac{Gb}{2\pi(1-\mu)R^2}\frac{Y}{\left(X^2+Y^2\right)^2}\left[\left(Y^2+2X^2\right)\left(R^2-\left(X^2+Y^2\right)\right)+X^2\left(R^2-3\left(X^2+Y^2\right)\right)\right], \tag{8}$$
$$\sigma_6 = \frac{Gb}{2\pi(1-\mu)R^2}\frac{X}{\left(X^2+Y^2\right)}\left[\left(\frac{X^2-Y^2}{X^2+Y^2}\right)-\left(R^2-\left(X^2+Y^2\right)\right)\right].$$

Eqs. (8) are reduced to Eqs. (3) when the sample radius R approaches to infinity and at the change of the Burgers vector component $\boldsymbol{b_2}$ to $\boldsymbol{b}_1$. In case of the Burgers vector parallel to the [010] axis, the reduced equations become as follows:

$$\sigma_1 = -\frac{Gb}{2\pi(1-\mu)}\frac{Y\left(X^2-Y^2\right)}{\left(X^2+Y^2\right)^2},\ \sigma_2 = \frac{Gb}{2\pi(1-\mu)}\frac{Y\left(3X^2+Y^2\right)}{\left(X^2+Y^2\right)^2},$$
$$\sigma_6 = \frac{Gb}{2\pi(1-\mu)}\frac{X\left(X^2-Y^2\right)}{\left(X^2+Y^2\right)^2}. \tag{9}$$

Now we wish to show that the core radius plays important role in the vicinity of the dislocation nucleus. As seen from Fig. 1, the stress tensor components σ_1 and σ_6 do not become infinite when the radial coordinate (or the X and Y coordinates) reaches the value r_0. Instead, the components σ_1 and σ_6 acquire some maximum value at $r > r_0$ and become zero when the radial coordinate is equal to the radius of the dislocation core ($r = r_0$). The component σ_2 remains finite at $r = r_0$, probably because the boundary conditions do not include the requirement $\sigma_2 = 0$ at $r = R$ and $r = r_0$. The dependences of the stress tensor components at $r < r_0$ have no physical meaning, since the dislocation core can be considered as some other phase. Finally, let us notice that

simplified Eqs. (3) and (9) yield non-physical solutions, the stress tensor components following to infinity under zeroing of the X and Y coordinates.

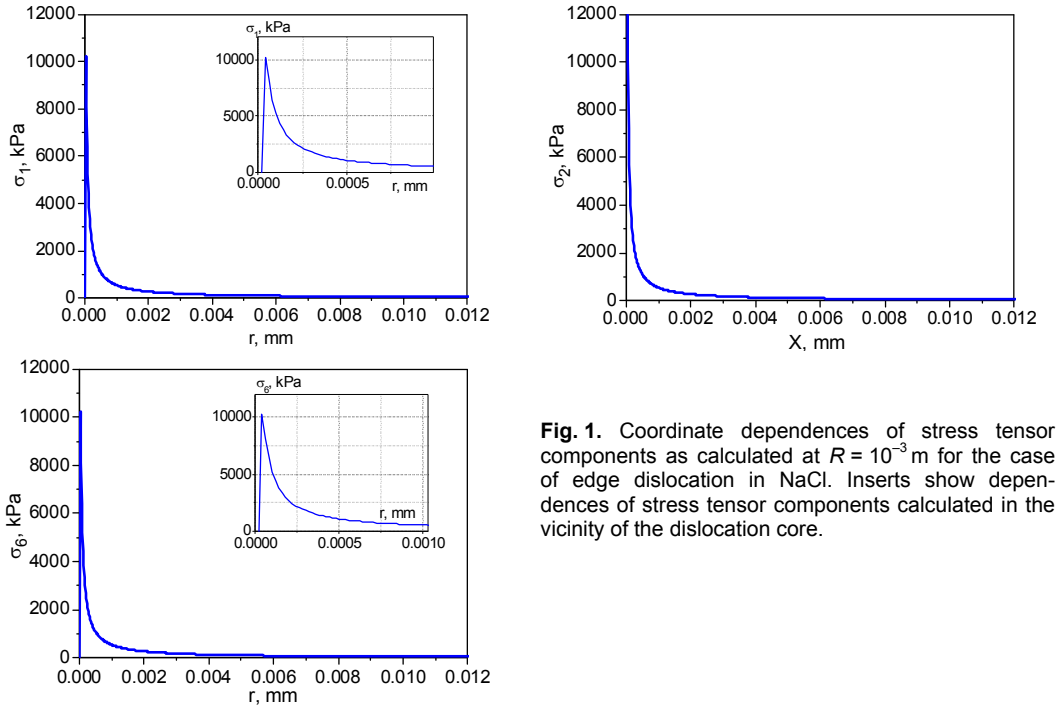

Fig. 1. Coordinate dependences of stress tensor components as calculated at $R = 10^{-3}$ m for the case of edge dislocation in NaCl. Inserts show dependences of stress tensor components calculated in the vicinity of the dislocation core.

While calculating the dependences displayed in Fig. 1, we have used the following parameters for the NaCl crystals: $G_1 = G_2 = G_3 = 11.8$ GPa and $\mu_1 = \mu_2 = \mu_3 = 0.028$, $S_{11} = 22.9\times10^{-12}\,\mathrm{m^2/N}$, $S_{12} = -4.8\times10^{-12}\,\mathrm{m^2/N}$ and $\pi_{11} = 1.27\times10^{-12}\,\mathrm{m^2/N}$, $\pi_{12} = 2.58\times10^{-12}\,\mathrm{m^2/N}$, $\pi_{44} = -0.84\times10^{-12}\,\mathrm{m^2/N}$, $n = 1.54$ (the refractive index at the light wavelength of $\lambda = 632.8$ nm), $R = 10^{-3}$ m, and $r_0 = 20$ nm (see Refs. [21–23]).

Using a standard matrix representation for the symmetric tensors, one can express the piezooptic effect in terms of the changes ΔB_i in the optical impermeability coefficients (or the refractive indices n_i, since $B_i = (1/n^2)_i$), which are imposed by the mechanical stresses σ_j [24]:

$$\Delta B_i = B_i - B_i^0 = \pi_{ij}\sigma_j\,. \tag{10}$$

Here π_{ij} is the fourth-rank piezooptic tensor, and B_i and B_i^0 the second-rank impermeability tensors of respectively stressed and free sample, which are written in the matrix form.

2.1. NaCl crystals

Let us begin with the NaCl crystals. If a wide light beam with almost plane front propagates along the Z axis, the birefringence and the angle of OI rotation induced piezooptically become as follows:

$$\Delta n_{12} = -\frac{n^3}{2}\sqrt{(\pi_{11}-\pi_{12})^2(\sigma_1-\sigma_2)^2 + 4\pi_{44}^2\sigma_6^2}\,,\ \tan 2\xi_3 = \frac{2\pi_{44}\sigma_6}{(\pi_{11}-\pi_{12})(\sigma_1-\sigma_2)}. \tag{11}$$

These equations are written for the component of the Burgers vector $\boldsymbol{b_2}$. After inserting Eqs. (7) for the mechanical stress tensor components into Eqs. (11), one readily obtains the *XY* spatial distribution of the birefringence and the angle of OI orientation shown in Fig. 2.

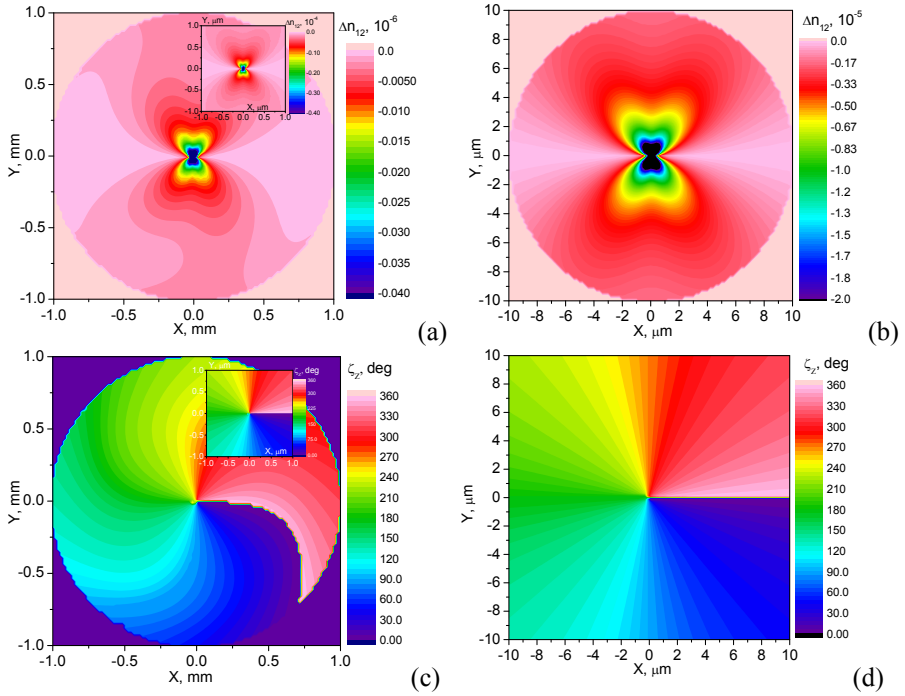

Fig. 2. *XY* distributions of birefringence (a, b) and angle of OI orientation (c, d, e) in NaCl calculated with Eqs. (7) and (11) (a, c) and simplified Eqs. (9) and (11) (b, d). Inserts show the same distributions calculated in the vicinity of the dislocation core.

As seen from Fig. 2, the *XY* distributions of the OI rotation calculated with Eqs. (7) and (11) are more complicated than those obtained using their simplified versions, Eqs. (9) and (11). Nonetheless, the strength of the TD of OI orientation located in the centre of the beam cross-section is equal to 1 in the both cases. In the vicinity of the dislocation core, the spatial distributions of the birefringence and the OI orientation calculated on the basis of Eqs. (7) and (11) become almost the same as those calculated with Eqs. (9) and (11).

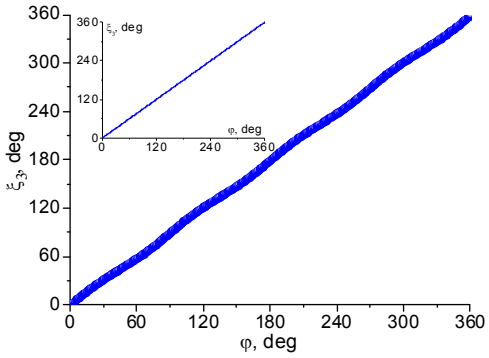

Fig. 3. Dependence of the angle of OI rotation around the Z axis on the tracing angle φ calculated for NaCl under the conditions of light propagation along the Z axis and r = R/2. Insert shows the same dependence calculated at r = 0.5 μm.

Let us assume that the coordinates *X* and *Y* approach the radius of the dislocation core and take into account that the stress component σ_2 should be zero at $r = r_0$ due to the boundary conditions (see Eqs. (7) and (11)). Then the birefringence has to become zero at $r = r_0$. This

corresponds to the exact conditions needed for generating a doubly charged optical vortex, i.e. a zero light intensity and an undefined phase of optical wave at $r = r_0$. The angle of OI rotation is then the same as the tracing angle φ. Moreover, as seen from Fig. 3, the dependence of the angle of OI rotation on the tracing angle is almost linear at $r = R/2$. On the other hand, it becomes exactly linear close to the dislocation core (see Fig. 3, insert). These facts imply the appearance of the TD of OI orientation, with the strength equal to 1, and a possibility for generating an almost canonical, doubly charged optical vortex.

2.2. $LiNbO_3$ crystals

\Let us now proceed to the case of $LiNbO_3$ crystals and write out the theoretical relations and the experimental data necessary for further analysis:

$$G_1 = G_2 = \frac{1}{S_{44}}, \quad G_3 = \frac{1}{2(S_{11} - S_{12})}, \quad \mu_1 = \mu_2 = -\frac{S_{12} + S_{13}}{2S_{11}}, \quad \mu_3 = -\frac{S_{13}}{S_{33}}, \qquad (12)$$

$\pi_{11} = -(0.376 \pm 0.069) \times 10^{-12}\,\mathrm{m}^2/\mathrm{N}$, $\pi_{12} = (0.197 \pm 0.039) \times 10^{-12}\,\mathrm{m}^2/\mathrm{N}$ and $\pi_{14} = (0.875 \pm 0.071) \times 10^{-12}\,\mathrm{m}^2/\mathrm{N}$ [25, 26], $S_{11} = 5.831 \times 10^{-12}\,\mathrm{m}^2/\mathrm{N}$, $S_{14} = -1.000 \times 10^{-12}\,\mathrm{m}^2/\mathrm{N}$, $S_{33} = 5.026 \times 10^{-12}\,\mathrm{m}^2/\mathrm{N}$, $S_{12} = -1.150 \times 10^{-12}\ \mathrm{m}^2/\mathrm{N}$, $S_{13} = -1.452 \times 10^{-12}\ \mathrm{m}^2/\mathrm{N}$ and $S_{44} = S_{44} = 17.10 \times 10^{-12}\ \mathrm{m}^2/\mathrm{N}$ [27], $G_1 = G_2 = 58.5$ GPa and $G_3 = 71.6$ GPa, $\mu_1 = \mu_2 = 0.223$ and $\mu_3 = 0.289$, $n_o = 2.28647$ (at $\lambda = 632.8$ nm), $R = 10^{-3}$ m, and $r_0 = 20$ nm. The birefringence and the angle of OI rotation read respectively as

$$\Delta n_{12} = -\frac{n_o^3}{2}\pi_{66}\sqrt{(\sigma_1 - \sigma_2)^2 + 4\sigma_6^2}, \quad \tan 2\xi_3 = \frac{2\sigma_6}{(\sigma_1 - \sigma_2)}, \qquad (13)$$

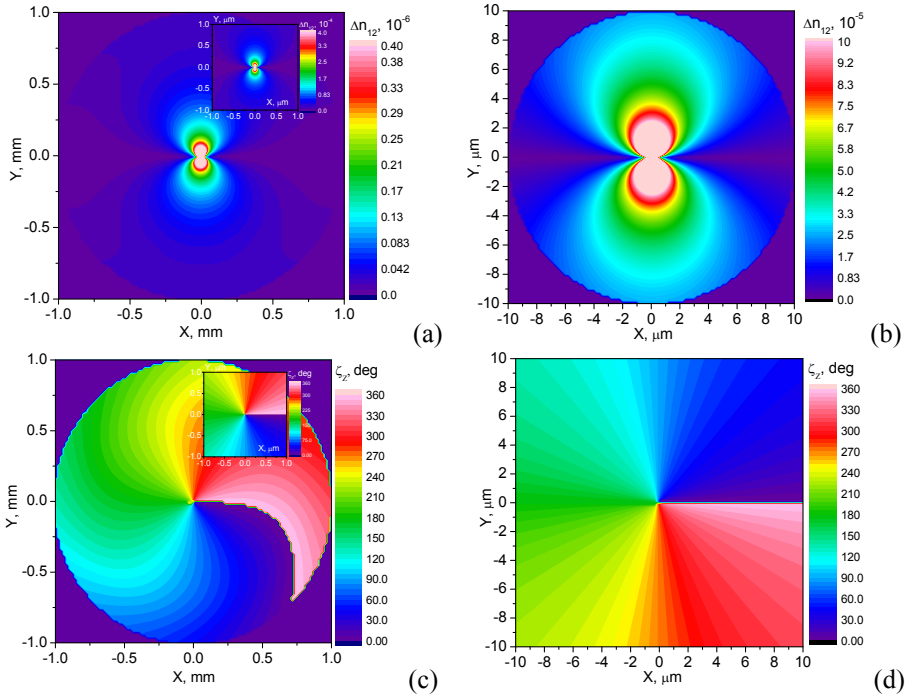

Fig. 4. *XY* spatial distributions of birefringence (a, b) and angle of OI orientation (c, d) in $LiNbO_3$ calculated with Eqs. (7) and (13) (a, c) and simplified Eqs. (9) and (13) (b, d). Inserts show the same distributions calculated in the vicinity of the dislocation core.

The strength of the TD of OI orientation for the $LiNbO_3$ crystals turns out to be the same as for the NaCl crystals. As seen from Fig. 4, the spatial distributions of the birefringence and the OI orientation calculated with Eqs. (7) derived after considering the boundary conditions are almost the same as those calculated using Eqs. (9), which neglect the boundary conditions. In the vicinity of the dislocation core, the birefringence in $LiNbO_3$ reaches the value of 4×10^{-4}. For achieving the phase difference $\Delta\Gamma = 2\pi\Delta n_{12} d / \lambda$ equal to π, at which the efficiency of the SAM-to-OAM conversion is maximal, a thin crystalline plate with the thickness d equal to ~ 0.8 mm is enough. Hence, optical observations of the edge dislocation in the polarized light using an optical microscope seem to be quite feasible. In particular, using a circularly polarized incident light and an orthogonal circular analyzer, one can easily observe the appearance of the optical vortices around the dislocation core.

3. Conclusions

In the present work we have analyzed the spatial inhomogeneity of the optical birefringence and the angle of OI rotation, which are induced by mechanical stresses caused by the structural edge dislocation. Cubic and tetragonal crystals have been exemplified by NaCl and $LiNbO_3$, respectively. In our simulation we have used relations for coordinate dependencies of stress tensor components derived with accounting of approximate boundary conditions.

We have found that accounting for the strict boundary conditions leads to zeroing of the stress tensor components and, subsequently, of the piezooptically induced birefringence in the vicinity of the dislocation core, thus meeting the exact conditions needed for the appearance of optical vortices, with a light ring located around the dislocation core. It is important that consistent consideration of the boundary conditions removes a non-physical solution, infinitely large mechanical stress components calculated for the case if the radial coordinate approaches the dislocation centre.

It follows from our analysis that the edge dislocation can easily be detected in the polarized light, using an optical microscope, even in the case when the Burgers vectors are small enough and the piezooptic coefficients acquire some intermediate values.

References

1. Skab I, Vasylkiv Yu, Zapeka B, Savaryn V and Vlokh R, 2011. On the appearance of singularities of optical field under torsion of crystals containing three-fold symmetry axes. J. Opt. Soc. Amer. A. **28**: 1331–1340.
2. Skab I, Vasylkiv Yu, Smaga I and Vlokh R, 2011. Spin-to-orbital momentum conversion via electrooptic Pockels effect in crystals. Phys. Rev. A. **84**: 043815.
3. Skab I, Vasylkiv Yu and Vlokh R, 2012. Induction of optical vortex in the crystals subjected to bending stresses. Appl. Opt. **51**: 5797–5805.
4. Skab I, Vasylkiv Yu, Krupych O, Savaryn V and Vlokh R, 2012. Generation of doubly charged vortex beam by concentrated loading of glass disks along their diameter. Appl. Opt. **51**: 1631–1637.
5. DiVincenzo D P, 1995. Quantum computation. Science. **270**: 255–261.
6. Groblacher S, Jennewein T, Viziri A, Weihs G and Zeillinger A, 2006. Experimental quantum cryptography with qutrits. New J. Phys. **8**: 75.
7. Molina-Terriza G, Vaziri A, Rehácek J, Hradil Z and Zeilinger A, 2004. Triggered qutrits for quantum communication protocols. Phys. Rev. Lett. **92**: 167903.
8. Bouwmeester D, Pan J-W, Mattle K, Eibl M, Weinfurter H and Zeilinger A, 1997. Experimental quantum teleportation. Nature. **390**: 575–579.
9. Grier D G, 2003. A revolution in optical manipulation. Nature. **424**: 810–816.

10. Soskin M and Vasnetsov M, 2001. Singular optics. Progr. Opt. **42**: 219–276.
11. Marrucci L, 2008. Generation of helical modes of light by spin-to-orbital angular momentum conversion in inhomogeneous liquid crystals. Mol. Cryst. Liq. Cryst. **488**: 148–162.
12. Marrucci L, Karimi E, Slussarenko S, Piccirillo B, Santamato E, Nagali E and Sciarrino F, 2011. Spin-to-orbital conversion of the angular momentum of light and its classical and quantum applications. J. Opt. **13**: 064001.
13. Karimi E, Piccirillo B, Nagali E, Marrucci L and Santamato E, 2009. Efficient generation and sorting of orbital angular momentum eigenmodes of light by thermally tuned q-plates. Appl. Phys. Lett. **94**: 231124.
14. Piccirillo B, D'Ambrosio V, Slussarenko S, Marrucci L and Santamato E, 2010. Photon spin-to-orbital angular momentum conversion via an electrically tunable q-plate. Appl. Phys. Lett. **97**: 241104.
15. Beth R A, 1936. Mechanical detection and measurement of the angular momentum of light. Phys. Rev. **50**: 115–125.
16. Savaryn V, Vasylkiv Yu, Krupych O, Skab I and Vlokh R, 2013. Polarization singularities of optical fields caused by structural dislocations in crystals. J. Opt. **15**: 044023.
17. Savaryn V, Vasylkiv Yu, Krupych O, Skab I and Vlokh R, 2015. Corrigendum: Polarization singularities of optical fields caused by structural dislocations in crystals (J. Opt. 2013, **15** 044023) J. Opt. **17**: 089501.
18. Likhachev V A and Khairov R Yu, Introduction into the theory of disclinations. Leningrad: Publishing House of Leningrad University (1975).
19. Friedel J, Dislocations. Oxford: Pergamon Press (1964).
20. Lurie A I and Belyaev A, Theory of elasticity. Berlin: Springer (2005)
21. Hellwege K-H and Hellwege A M, Landolt–Börnstein numerical data and functional relationships in science and technology, New Series, Group III: Crystal and solid state physics, Vol.11: Elastic, piezoelectric, pyroelectric, piezooptic, electrooptic constants and nonlinear susceptibilities of crystals. Berlin: Springer-Verlag (1979).
22. http://www.elektrosteklo.ru/NaCl_rus.htm
23. http://www.optotl.ru/mat/NaCl
24. Narasimhamurty T S, Photoelastic and electrooptic properties of crystals. New York: Plenum Press (1981).
25. Krupych O, Savaryn V and Vlokh R, 2014. Precise determination of full matrix of piezo-optic coefficients with a four-point bending technique: the example of lithium niobate crystals. Appl. Opt. **53**: B1–B7.
26. Vasylkiv Yu, Savaryn V, Smaga I, Skab I and Vlokh R 2011 On determination of sign of the piezo-optic coefficients using torsion method. Appl. Opt. **50**: 2512–2518.
27. Weis R S and Gaylord T K 1985 Lithium niobate: Summary of physical properties and crystal structure. Appl. Phys. A. **37**: 191–203.

Savaryn V, Vasylkiv Yu, Skab I and Vlokh R. 2015. Topological defects of optical indicatrix orientation associated with the edge structural dislocations in crystals. Ukr.J.Phys.Opt. **16**: 138–146.

Анотація. *У роботі проаналізовано вплив крайових структурних дислокацій у кристалах на топологію параметрів оптичної індикатриси. Показано, що врахування строгих граничних умов приводить до занулення компонент тензора механічних напружень і, як наслідок, оптичного двопроменезаломлення в околі серцевини дислокації, забезпечуючи точні умови для генерації оптичних вихорів зі світловим кільцем навколо ядра дислокації. Продемонстровано, що навіть за умов малих векторів Бюргерса і невеликих значень п'єзооптичних коефіцієнтів крайові дислокації можна виявити в поляризованому світлі з використанням оптичного мікроскопа.*